Supplement of Atmos. Chem. Phys., 15, 3241–3255, 2015
http://www.atmos-chem-phys.net/15/3241/2015/
doi:10.5194/acp-15-3241-2015-supplement

Atmospheric Chemistry and Physics
Open Access

Supplement of

Spaceborne observations of the lidar ratio of marine aerosols

K. W. Dawson et al.

Correspondence to: N. Meskhidze (nmeskhidze@ncsu.edu)

Supplementary Information

Table S1. Common techniques for measuring the lidar ratio along with some values reported for marine aerosol at, or near, 532 nm wavelength.

Instrumentation	Type	Operating Principle	$S_{p,532}$ (sr)
Raman Lidar[b]	Direct	Light is scattered at a different wavelength than the incident laser. Aerosol extinction is calculated by the Raman lidar equation. Rayleigh coefficients for molecular attenuation are calculated with measured or modeled temperature and pressure profiles. The ratio of inelastic (shifted wavelength due to aerosol scattering) backscatter to the elastic (same wavelength) backscatter determines the aerosol backscatter. The particulate lidar ratio is then the aerosol extinction-to-backscatter.	23 ± 3[a] 23 ± 5[a] 18 ± 2[c,d]
HSRL Lidar[h]	Direct	The HSRL technique relies on the difference in spectral distribution of backscattered signal from molecules and particulates. Discrimination between aerosol/cloud and molecular returns in the receiver is accomplished by splitting the returned signal into two optical channels: the molecular backscatter channel, which is equipped with an extremely narrowband iodine vapor absorption filter to eliminate the aerosol returns and pass the wings of the molecular spectrum, and the total backscatter channel, which passes all frequencies of the returned signal. After appropriate internal calibration of the sensitivities of the two channels, the signals are used to derive profiles of extinction, backscatter coefficient, and extinction-to-backscatter ratio, S_p.	18 ± 5[e] $15 - 25$[f] $17 - 27$[g]
Modeled with measured size distributions[i]	Indirect	The aerosol size distribution is measured and used with Mie theory (with an assigned or measured refractive index) to retrieve aerosol extinction and backscatter and thereby the lidar ratio. AERONET (Holben et al., 1998) uses an inversion procedure from radiance data collected by sun photometers to derive the aerosol size distribution.	28*[i] 25.4 ± 3.5[j] 29+[k]
Phase function and single scattering albedo measurements[l]	Indirect	The lidar ratio is also written as the inverse of the single scattering albedo and phase function at 180°. Passive instruments like the POLarization and Directionality of the Earth's Reflectances (POLDER) radiometer retrieve aerosol scattering at multiple angles to determine the phase function and retrieve the lidar ratio. This can also be done with lidar and backscattering nephelometers.	25[l] 21.3 ± 3.7§[m]

- [a]Müller et al. (2007); [b] Ansmann and Müller (2005); [c,d,e] Groß et al. (2011a; 2011b; 2013); [f,g] Burton et al. (2012; 2013); [h] Hair et al. (2008); [i] Sayer et al. (2012); [j] Masonis et al. (2003); [k] Cattrall et al. (2005); [l] Bréon (2013); [m]Doherty et al. (1999). * signifies a suggested value, + signifies 550 nm and § refers to a nephelometer study where extinction and backscatter were separately measured.
- Direct retrievals are those that measure aerosol extinction and backscatter explicitly. Indirect retrievals are those that rely on inversion algorithms, size distribution assumptions (find/coarse mode partitioning), chemical composition assumptions (i.e. refractive index), etc. to back out the lidar ratio from retrieval results (this study is an indirect method for determining the lidar ratio).

SODA/MAN Comparison

Daytime SODA data for the time period of 2007-2010 are compared to the Maritime Aerosol Network (MAN; Smirnov et al., 2009) observations of aerosol optical depth (AOD). The MAN observations are made with handheld sunphotometers on ships and report the AOD at a number of wavelengths. In order to most accurately reference the MAN observations to the SODA retrievals of AOD, we corrected MAN AOD at 500 nm to 532 nm by the 500/675 nm angstrom exponent. Then we employed the colocation scheme from Smirnov et al. (2011) and Kleidman et al. (2010). In brief, the colocation scheme required the closest SODA overpass within ± 30 minutes of the MAN measurement and no more than 25 km in radius from the ship. The results are presented below in supplementary Fig. S1. There were 51 matches in total in 6 locations for the selected measurement period. Points with fewer than 2 MAN retrievals have not been included in the scatterplot (Fig. S1 b).

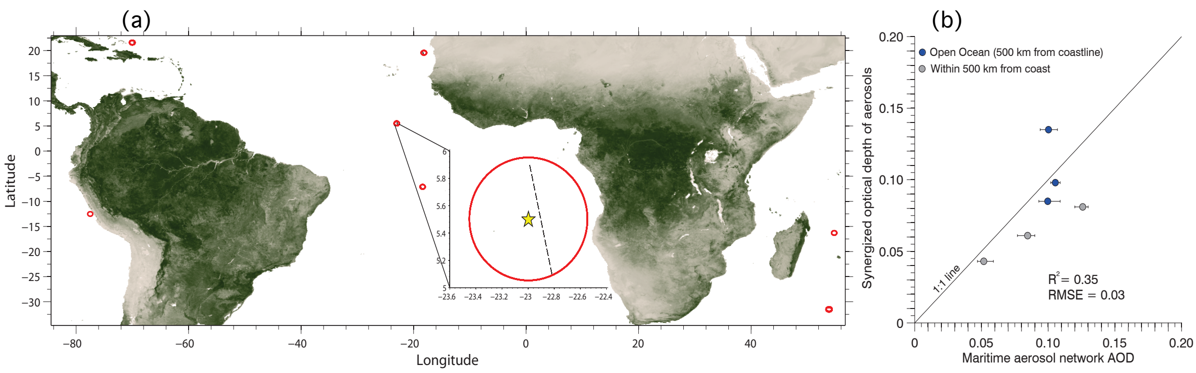

Fig S1. Map of collocated instances for SODA and MAN measurements of aerosol optical depth. (a) Red circles indicate the region where a satellite track resides and the inset displays the satellite track (dashed line) in comparison to the MAN measurement (yellow star). Scatter plot comparing closest SODA to mean MAN aerosol optical depth. (b) The error bars indicate the range of MAN reported AOD within a ± 30 minute SODA overpass. The R^2 and RMSE are also shown. Blue circles indicate points at least 500 km from the nearest coastline.

SODA CALIPSO comparison of aerosol optical depth

Figure S2 shows scatter density plots (Fig. S2a) along with the distribution of errors (Fig. S2b,c). These plots compare the grid cell medians for all of the data used in the manuscript and total 13,481 points. The distribution of errors show that the RMS error is 0.06. Redemann et al. (2012) stated that for RMS error < 0.1, the combination of instruments can be used to obtain further information on aerosol optical properties. The distribution of errors is evaluated to obtain the median error of 47%. The CALIOP retrieved AOD is directly a function of the prescribed lidar ratio and is a major contributor to the bias shown in Fig. S2 (a). An increase in the prescribed lidar ratio would mitigate some of this bias.

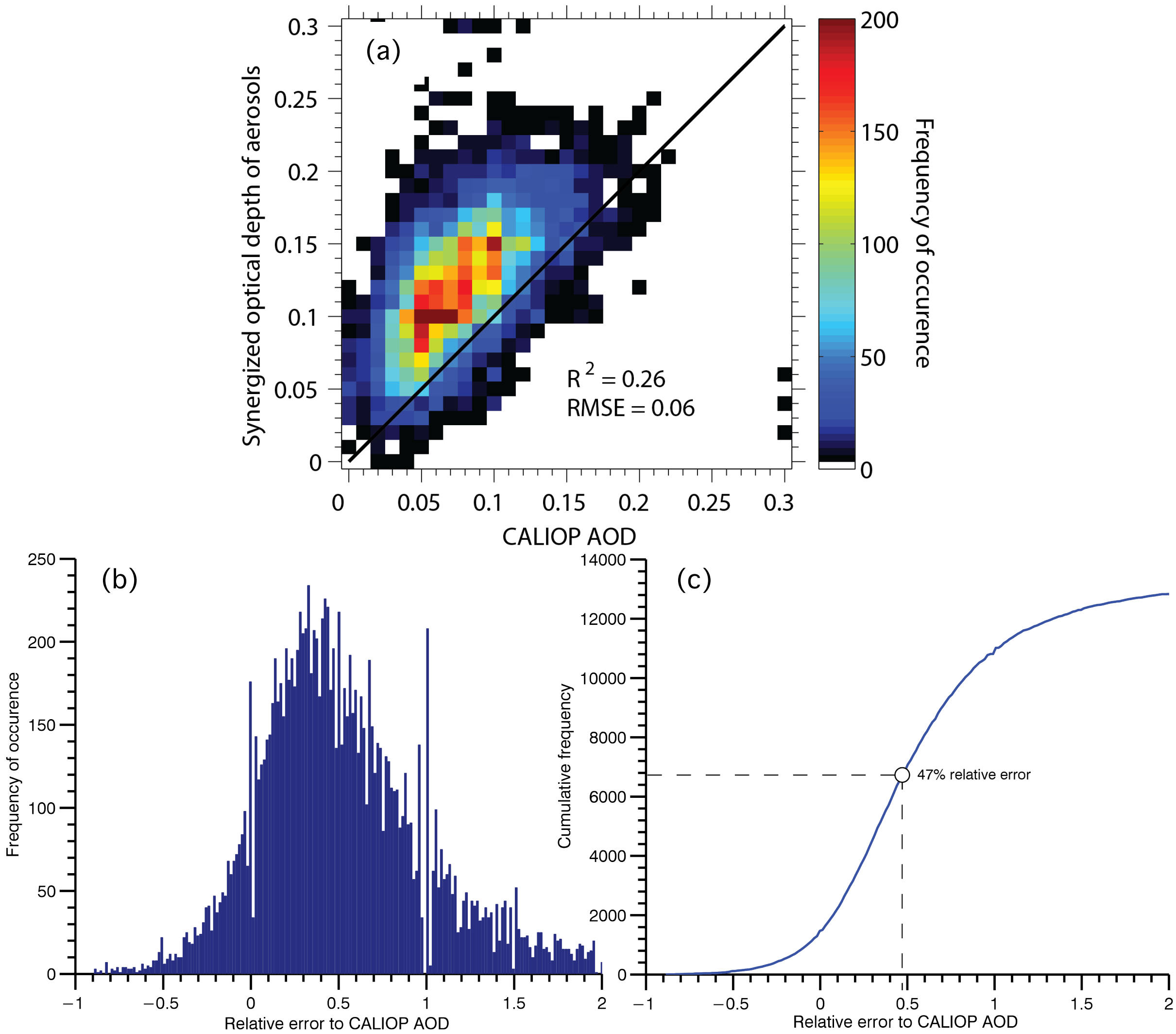

Fig. S2. (a) Scatter density plot of all available (13,481 occurences) SODA to CALIOP aerosol optical depth data. Each point indicates a grid cell median from the spatial maps shown in the main manuscript. The solid black line is the 1:1 relation. The R^2 value is 0.26 and the RMS error is 0.06. (b) Histogram of the relative error of SODA compared to CALIOP for each of the points indicated in (a). (c) Cumulative error with the median value reported at 47%.

References

Ansmann, A. and Múller, D.: Lidar and Atmospheric Aerosol Particles, in: Lidar, Weitkamp, C. (Ed.), Springer New York, 105-141, 2005.

Bréon, F. M.: Aerosol extinction-to-backscatter ratio derived from passive satellite measurements, Atmos. Chem. Phys., 13, 8947-8954, doi:10.5194/acp-13-8947-2013, 2013.

Burton, S. P., Ferrare, R. A., Vaughan, M. A., Omar, A. H., Rogers, R. R., Hostetler, C. A., and Hair, J. W.: Aerosol classification from airborne HSRL and comparisons with the CALIPSO vertical feature mask, Atmos. Meas. Tech., 6, 1397-1412, doi:10.5194/amt-6-1397-2013, 2013.

Burton, S., Ferrare, R., Hostetler, C., Hair, J., Rogers, R., Obland, M., Butler, C., Cook, A., Harper, D. and Froyd, K.: Aerosol classification using airborne High Spectral Resolution Lidar measurements–methodology and examples, Atmos. Meas. Tech., 5, 73-98, doi:10.5194/amtd-4-5631-2011, 2012.

Cattrall, C., Reagan, J., Thome, K. and Dubovik, O.: Variability of aerosol and spectral lidar and backscatter and extinction ratios of key aerosol types derived from selected Aerosol Robotic Network locations, J. Geophys. Res., 110, D10S11, doi:10.1029/2004JD005124, 2005.

Doherty, S. J., Anderson, T. L. and Charlson, R. J.: Measurement of the lidar ratio for atmospheric aerosols with a 180 backscatter nephelometer, Appl. Opt., 38, 1823-1832, 1999.

Groß S., Esselborn, M., Weinzierl, B., Wirth, M., Fix, A. and Petzold, A.: Aerosol classification by airborne high spectral resolution lidar observations, Atmos. Chem. Phys., 13, 2487-2505, doi:10.5194/acp-13-2487-2013, 2013.

Groß S., Tesche, M., Voker, F., Toledano, C., Wiegner, M., Ansmann, A., Althausen, D., Seefeldner,M.: Characterization of Saharan dust, marine aerosols and mixtures of biomass-burning aerosols and dust by means of multi-wavelength depolarization and Raman lidar measurements during SAMUM 2, Tellus B, 63, 706-724, doi:10.1111/j.1600-0889.2011.00556.x, 2011b.

Groß, S., Gasteiger, J., Freudenthaler, V., Wiegner, M., Geiß, A., Schladitz, A., Toledano, C., Kandler, K., Tesche, M., Ansmann, A. and Wiedensohler, A.: Characterization of the planetary boundary layer during SAMUM-2 by means of lidar measurements, Tellus B, 63, 695-705, doi:10.1111/j.1600-0889.2011.00557.x, 2011a.

Hair, J. W., Hostetler, C. A., Cook, A. L., Harper, D. B., Ferrare, R. A., Mack, T. L., Welch, W., Izquierdo, L. R. and Hovis, F. E.: Airborne High Spectral Resolution Lidar for profiling aerosol optical properties, Appl. Opt., 47, 6734-6752, doi:10.1364/AO.47.006734, 2008.

Kleidman, R.G., Smirnov, A., Levy, R.C., Mattoo, S., Tanre, D.: Evaluation and Wind Speed Dependence of MODIS Aerosol Retrievals Over Open Ocean, *IEEE T Geosci Remote*, vol.50, no.2, pp.429,435, Feb. 2012, doi:10.1109/TGRS.2011.2162073, 2010.

Masonis, S. J., Anderson, T. L., Covert, D. S., Kapustin, V., Clarke, A. D., Howell, S. and Moore, K.: A Study of the Extinction-to-Backscatter Ratio of Marine Aerosol during the Shoreline Environment Aerosol Study, J. Atmos. Ocean. Technol., 20, 1388-1402, doi:10.1175/1520-0426(2003)020<1388:ASOTER>2.0.CO;2, 2003.

Müller, D., Ansmann, A., Mattis, I., Tesche, M., Wandinger, U., Althausen, D. and Pisani, G.: Aerosol-type-dependent lidar ratios observed with Raman lidar, J. Geophys. Res., 112, 10.1029/2006JD008292, 2007.

Redemann, J., Vaughan, M. A., Zhang, Q., Shinozuka, Y., Russell, P. B., Livingston, J. M., Kacenelenbogen, M., and Remer, L. A.: The comparison of MODIS-Aqua (C5) and CALIOP (V2 & V3) aerosol optical depth, Atmos. Chem. Phys., 12, 3025-3043, doi:10.5194/acp-12-3025-2012, 2012.

Sayer, A., Smirnov, A., Hsu, N. and Holben, B.: A pure marine aerosol model, for use in remote sensing applications, J. Geophys. Res., 117, doi:10.1029/2011JD016689, 2012.

Smirnov, A., Holben, B. N., Giles, D. M., Slutsker, I., O'Neill, N. T., Eck, T. F., Macke, A., Croot, P., Courcoux, Y., Sakerin, S. M., Smyth, T. J., Zielinski, T., Zibordi, G., Goes, J. I., Harvey, M. J., Quinn, P. K., Nelson, N. B., Radionov, V. F., Duarte, C. M., Losno, R., Sciare, J., Voss, K. J., Kinne, S., Nalli, N. R., Joseph, E., Krishna Moorthy, K., Covert, D. S., Gulev, S. K., Milinevsky, G., Larouche, P., Belanger, S., Horne, E., Chin, M., Remer, L. A., Kahn, R. A., Reid, J. S., Schulz, M., Heald, C. L., Zhang, J., Lapina, K., Kleidman, R. G., Griesfeller, J., Gaitley, B. J., Tan, Q., and Diehl, T. L.: Maritime aerosol network as a component of AERONET – first results and comparison with global aerosol models and satellite retrievals, *Atmos. Meas. Tech.*, 4, 583-597, doi:10.5194/amt-4-583-2011, 2011.

Smirnov, A., Holben, B. N., Slutsker, I., Giles, D. M., McClain, C. R., Eck, T. F., Sakerin, S. M., Macke, A., Croot, P., Zibordi, G., Quinn P. K., Sciare, J., Kinne, S., Harvey, M., Smyth, T. J., Piketh S., Zielinski, T., Proshutinsky A., Goes, J. I., Nelson, N. B., Larouche, P., Radionov, V. F., Goloub, P., Krishna Moorthy, K., Matarrese, R., Robertson, E. J. and Jourdin, F.: Maritime Aerosol Network as a component of Aerosol Robotic Network, J. Geophys. Res., 114, D06204, doi:10.1029/2008JD011257, 2009.